DESIGN OF A GENERIC WING MODEL FOR BASIC STALL PHENOMENA

F. Moëns
ONERA – The French Aerospace Lab, Meudon (France), frederic.moens@onera.fr, +33 (0)1 4673 4211

Abstract

Loss of control is the major source of accident for commercial transports and general aviation, and stall is about one third of them. The prediction and control of stall is therefore a major stake for flight safety. However, stall mechanisms occurring on aircraft are of high complexity, as they generally combine different mechanisms leading to the boundary layer separation, depending on local flow characteristics. Recent developments on numerical methods make possible the vision of an accurate prediction of stall in a near future, but to reach this objective, there is a need of high quality experimental database, including flow field measurements, for validation. A research program for the prediction, analysis and control of wing stall has been led at ONERA for a better understanding and prediction of basic physical phenomena leading to stall. This program, named PANDA (French acronym for Prévision et ANalyse du Décrochage d'Aile) considers both experimental and numerical aspects. Within the different work packages of the project, one considers a generic wing at low speed conditions, aiming at building up experimental database for basic stall phenomena, mainly trailing-edge and leading-edge stall. The paper presents the design process, by the use of RANS method, of the wing-body model dedicated to this task. The NACA4412 airfoil has been selected as basic airfoil for wing generation. A first step of the design process considers a half-wing model, which twist has been adapted in order to have a quasi bi-dimensional trailing-edge separation close to stall. Then, a generic "fuselage" has been adapted to this wing and designed in order to recover the flow characteristics observed for the half-wing model. Finally, the effect of the wing sweep angle has been evaluated, and numerical results have been used for the equipment definition in term of steady and unsteady pressure sensors.

Introduction

Loss of control in flight is the major source of accident for commercial transport and general aviation, and stall is about one third of them [1][2][3]. The prediction and control of stall is therefore a major stake for flight safety. However, stall mechanisms occurring on aircraft are of high complexity and depend on the flight conditions. At low speed, wing stall is caused by a boundary layer separation that propagates from trailing-edge or that occurs at leading-edge. When considering high-lift systems deployed at take-off or landing, the wing stall is driven by stall occurrence on the front elements (slat, main wing) depending on local flow conditions and on geometrical details. At transonic cruise speed, stall occurs beyond buffet onset and leads to unusual flow conditions. Finally, when considering real accident data, the aerodynamic flow conditions encountered are generally not covered by conventional tests, which makes the airplane behavior not known in these conditions (see for example Figure 1, from [4]).

Whatever the flight condition are, a good capability for stall prediction and its characterization in post-stall conditions would therefore improve the aircraft design and give flight mechanics inputs for stall recovery systems. In the past, several research activities on stall considered helicopter rotors or airfoils, but very few for generic aircraft configurations. Meantime, numerical methods have improved their prediction capabilities for the computation of unsteady flow (turbulence models, Hybrid RANS/LES, LES …) and non intrusive experimental measuring techniques are more and more routinely used in installations.

In 2018, ONERA launched an internal research program for the prediction, analysis and control of wing stall, with the aim of a better understanding and prediction of basic physical phenomena leading to stall

through simulations and experiments using most recent numerical tools (for prediction) and experimental measuring techniques (for analysis).

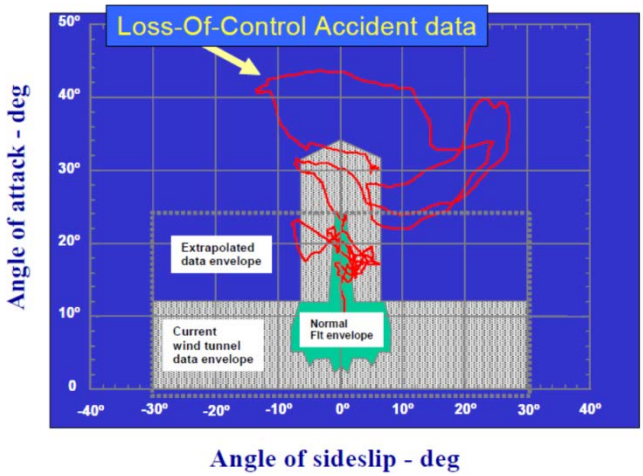

Figure 1 : Transport aircraft loss of control accident data relative to incidence and sideslip angles.

This program named PANDA (French acronym for Prévision et ANalyse du Décrochage d'Aile / Prediction and Analysis of Wing Stall) considers different work packages dealing with different flow physics: pre-stall, stall and post stall. Among the different tasks, one considers a generic wing at low speed conditions aiming at building up experimental database for basic stall phenomena (mainly trailing-edge and leading edge stalls), to be used for numerical prediction. This paper describes the design phase of this generic model, dedicated to basic stall phenomena study, by the use of CFD numerical tools.

Baseline characteristics of the model

The baseline airfoil considered for the generic wing is the NACA 4412. A NACA shape generator, based on the analytical relationships for NACA 4 digits airfoil [5], has been used to generate the NACA4412 airfoil to be used in all the different work packages of the PANDA project. Figure 2 compares the geometry obtained with the reference data from [6]. It can be seen that the curves obtained from the generator fits with the original data, particularly at the leading edge.

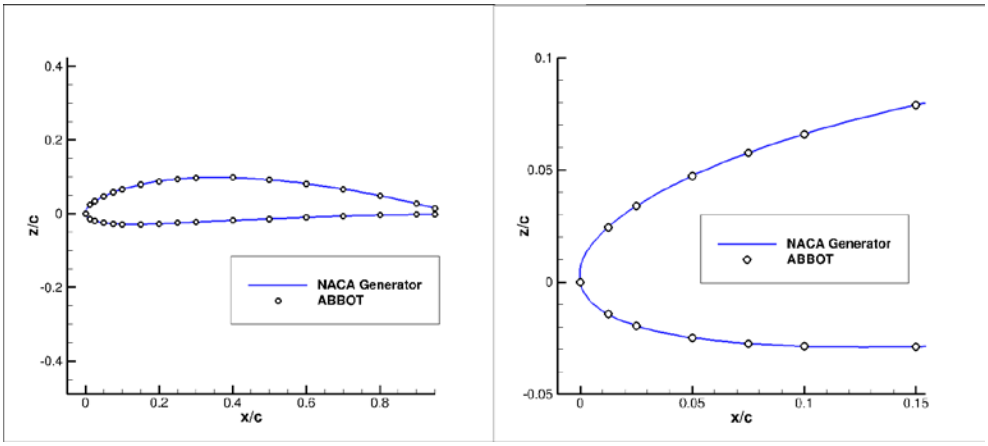

Figure 2 : NACA 4412 airfoil.

The wind tunnel selected is the ONERA-F2 low speed atmospheric wind tunnel, with a 1.5m×1.8m test section. The tunnel speed can be continuously varied from 0 to 100m/s. The typical speed foreseen for the tests is 50m/s. Test set up will consider a wing mounted on a vertical side wall, leading to a maximum

half-span of 1m for the model (from wall to tip). In order to set the main dimensions of the model, a compromise between a significant wing aspect ratio and Reynolds number, combined with an airfoil thickness that allows to fit the equipment has to be found. The following table presents the different characteristics corresponding to a rectangular wing with 1m for half-span and 12% of relative thickness.

AR	6.00	6.50	6.67	**7.00**	7.50
Chord (mm)	333.3	307.7	300.0	**285.7**	266.7
Thickness (mm)	40.0	36.9	36.0	**34.3**	32.0
Re_C (V=50 m/s)	$1.054\ 10^6$	$0.974\ 10^6$	$0.949\ 10^6$	**$0.904\ 10^6$**	$0.844\ 10^6$

The wing with an aspect ratio of 7.00 has been considered as a good compromise and has been retained for the model design. Of course, these values can be slightly modified by the workshop if there is a need for a small change in some dimensions for any practical reasons.

CFD solver used and Grids generated

The CFD solver used in this study is the elsA (v3.8.03) solver [7]. The elsA software (ONERA-Airbus-Safran property) solves the compressible three-dimensional RANS equations by using a cell-centered finite volume spatial discretization on structured multi-block meshes. For the spatial scheme, the one proposed by Jameson [8] is used for the conservative variables. A fourth order linear dissipation k_4 is generally used, with added second order dissipation terms k_2 for treatment of flow discontinuities. In the present study, k_2 was set to zero due to the low free stream Mach number, and the fourth order dissipation was set to k_4=0.016. The turbulence model used for the design phase is the one equation Spalart-Allmaras model [9] with the Quadratic Constitutive Relation (QCR) modification [10]. For the implicit stage, a LUssor scheme is associated with an Euler backward time integration scheme, which allows fast convergence rates. For the turbulent variables, an extension to the second order of the Roe numerical scheme is used with a Harten entropic correction coefficient set to 0.01 and the "minmod" limiter. Finally, multi-grid computations and low-speed preconditioning have been used for convergence acceleration.

The meshes used for the aerodynamic computations have been generated with the ICEM-CFD commercial software [11]. Two sets of computations have been considered in the design process: wing at wall or wing-body. Figure 3 presents the surface grids considered for both cases. Note that for the wing at wall cases, a portion of the symmetry plane has been considered as a viscous wall, in order to have a correct turbulent distance computation at the junction.

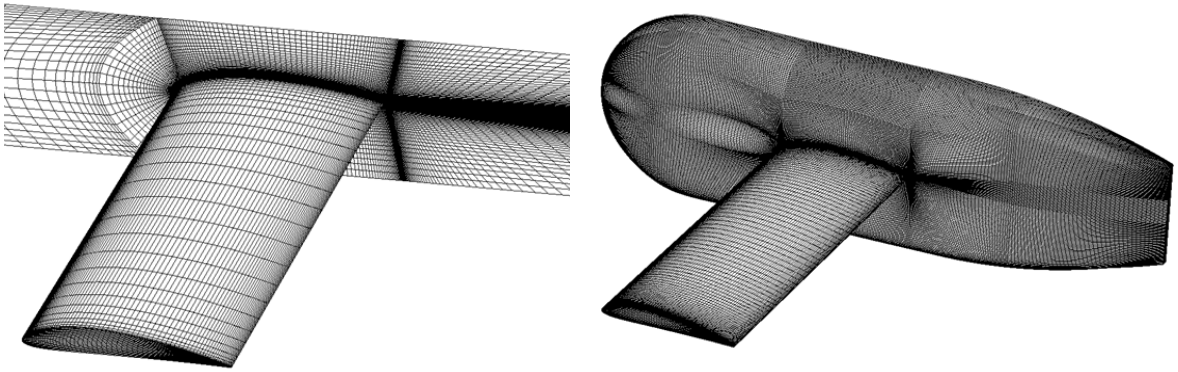

Wing at wall (7.5×10^6 nodes) Wing+Body (14×10^6 nodes)

Figure 3 : Surface grids for configurations considered.

Model design

For the design phase, the following characteristics have been used for all the computations presented:

- Computations in steady RANS approach;
- V=50m/s in atmospheric conditions (Re_C=0.904 10^6);
- Flow is assumed turbulent;
- Turbulent model used: Spalart-Allmaras + QCR correction.

Design Phase I: Wing at wall

For the first step, a rectangular wing untwisted has been considered for computations, and its characteristics evaluated up to and beyond maximum lift. A trailing-edge separation stall is found for that wing, but with some three-dimensional flow characteristics as it can be seen in Figure 4-left. For the purpose of the PANDA program, a more two-dimensional behavior is required. To do that, the twist at root has been decreased, in order to decrease the load, whereas twist at tip has been increased, in order to extent the separation line in tip area. Between the tip and root sections, a linear variation of twist is applied. The final design is presented in Figure 4-right with the computed separation line. The corresponding span loadings are compared in Figure 5. When comparing with the initial status, the flow separation can be considered as two dimensional on about 75% of wing span up to stall angle.

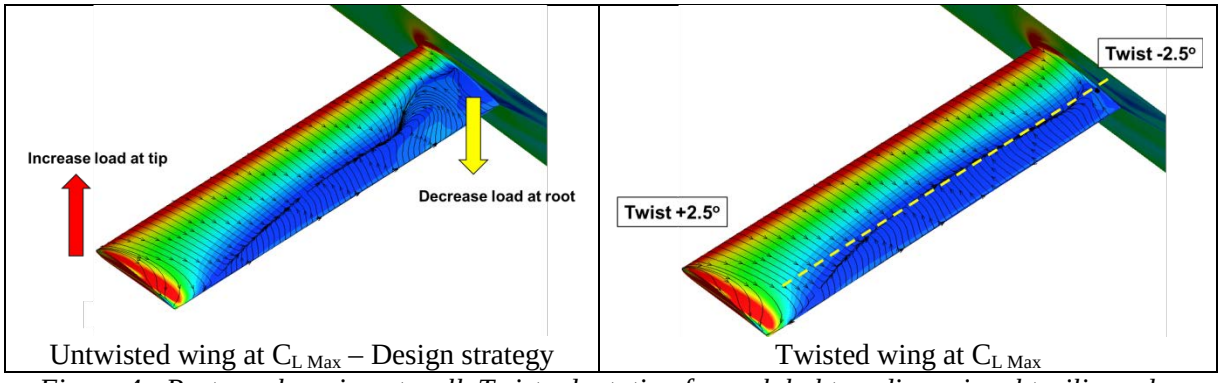

Untwisted wing at $C_{L\,Max}$ – Design strategy | Twisted wing at $C_{L\,Max}$

Figure 4 : Rectangular wing at wall. Twist adaptation for a global two dimensional trailing-edge separation at maximum lift (α=17.5°).

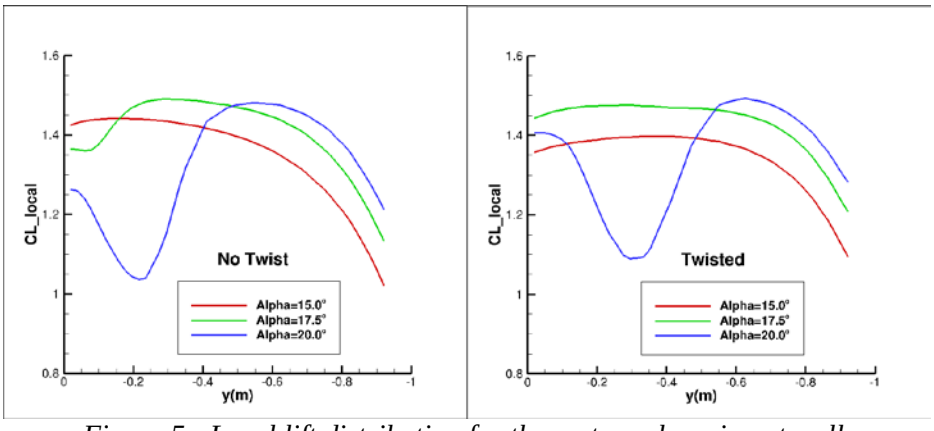

Figure 5 : Local lift distribution for the rectangular wing at wall.

Figure 6 presents the computed stall behavior of the twisted wing, from α=12.5° to 25°. Up to maximum lift (α=17.5°), a quasi two-dimensional trailing-edge separation is developed. Beyond maximum lift, a

stall cell seems to be present and its size increases spanwise, up to a complete separation on the wing suction side at $\alpha=25^{o}$.

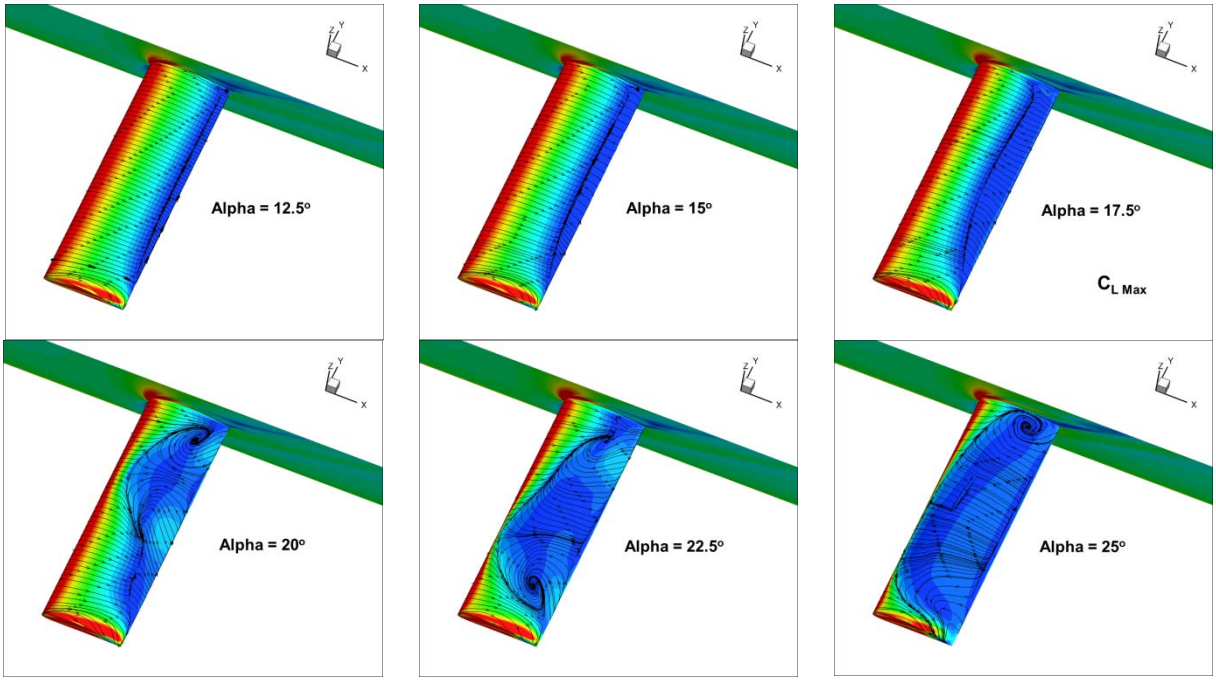

Figure 6 : Stall behavior of the twisted rectangular wing.

Design Phase II: Fuselage

It is planned to use a wing-body configuration for the test, in order to keep the wing outside the boundary layer of the tunnel wall. Additionally, the model has to consider different modular aspects, such as the use of different sweep angles and of high-lift devices. The body can be used to fit some mechanical devices or equipment that may not fit in the tunnel set up. Finally, it has to be checked that the flow topology of the wing-body configuration does not differ too much from the wing-at-wall case.

The "fuselage" used as reference shape is the one of the NASA Trap-Wing high-lift configuration, available on the HLPW-1 public website [12], where some IGES files of this configuration are available for grid generation. Then, different fuselages have been generated by applying different scaling factors on x/y/z directions, keeping constant the distance from tunnel wall and wing junction at 0.10m (Figure 8).

Figure 7 : NASA Trap-Wing model and its « fuselage » (from [12]).

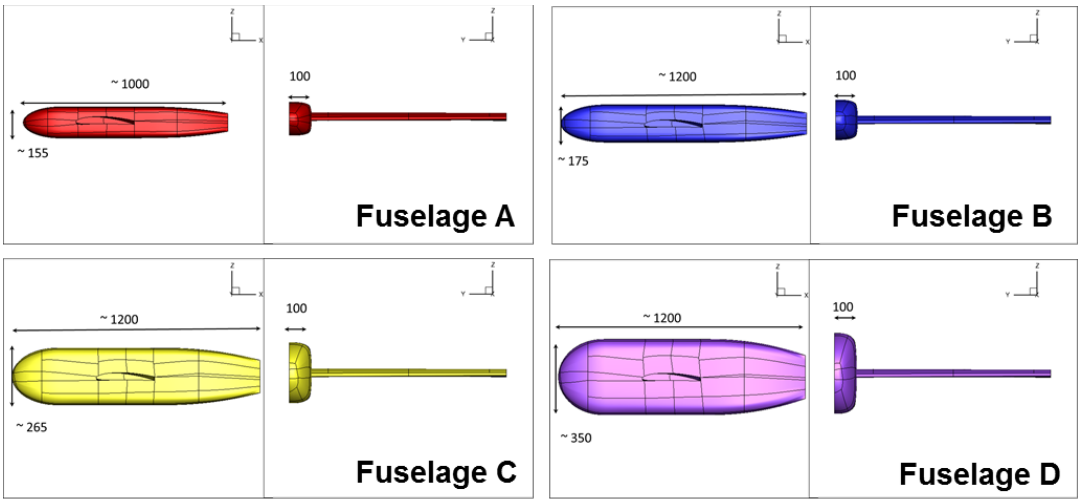

Figure 8 : The different fuselages considered for selection (dimensions in mm).

For the fuselage selection, the flow has been computed at $\alpha=15^{o}$, and compared to the solution obtained for the wing at wall configuration. Figure 9 presents the computed flow topology for the four fuselages considered. Increasing the height of the fuselage face tends to make the flow close to the wing at wall status by decreasing the size of the separation at wing fuselage junction. For the fuselage "D", this separation is almost removed, but still present. One possibility could be to create a new fuselage with a larger height size, 500/600 mm, but in that case its size could be significant with respect to the tunnel side wall. It was preferred to select the fuselage "D" and to make a final adaptation of the wing twist at root.

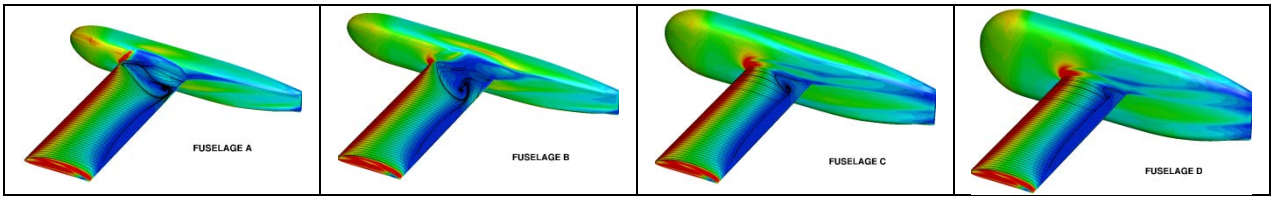

Figure 9 : Effect of fuselage dimensions on flow characteristics for $\alpha=15^{o}$.

This final process is presented in Figure 10 where the computed friction lines at maximum lift ($\alpha=17.5^{o}$) of the reference wing at wall configuration are compared with wing-fuselage D cases for different airfoil twist at the symmetry plane. When decreasing the airfoil twist inboard, there is a significant decrease of the separation at junction, up to a quite comparable status with the wing at wall case for a twist of -4.5^{o}.

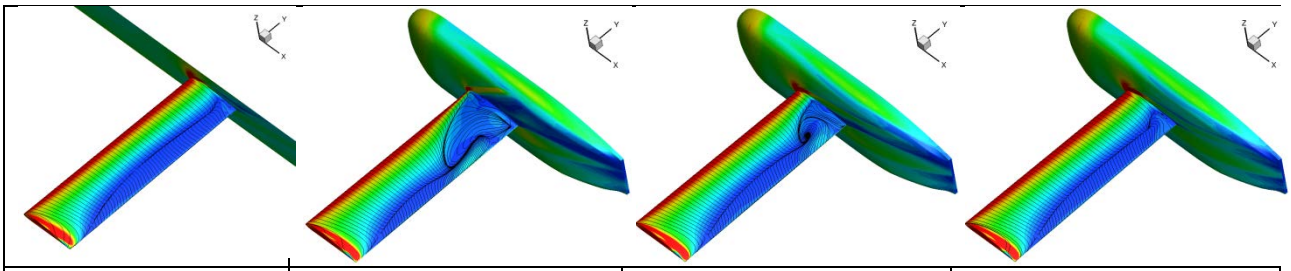

Wing at wall (Reference)	Fuselage D + Twist -2.5^{o} at symmetry plane	Fuselage D + Twist -3.5^{o} at symmetry plane	Fuselage D + Twist -4.5^{o} at symmetry plane

Figure 10 : Final adaptation of wing twist ($\alpha=17.5^{o}$).

This configuration has been retained as the reference one for the model. Figure 11 gives an overview of the corresponding main dimensions.

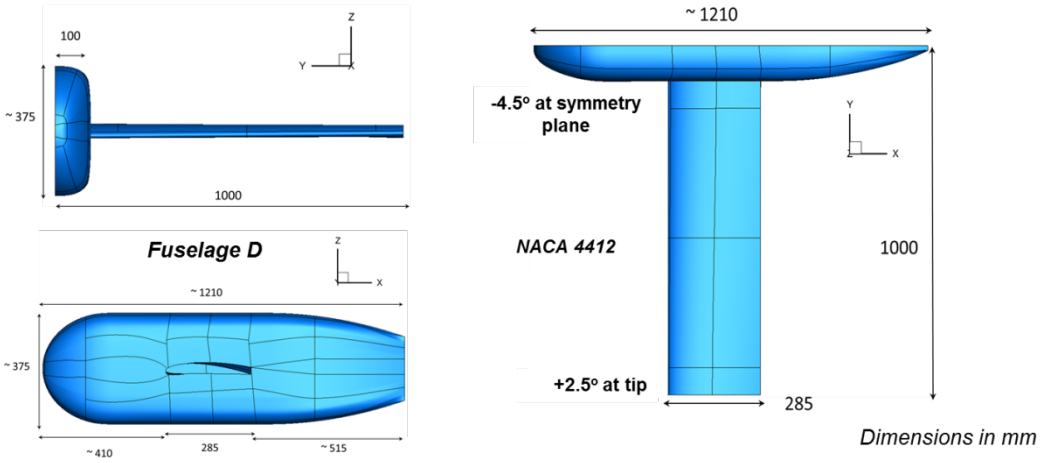

Figure 11 : General layout of the PANDA model.

Effect of turbulence model on computed performance

At this stage of the project, it is not necessary to evaluate a large number of models, as it will be part of the work plan when tests results will be validated. However, as the design process considered only one turbulence model (Spalart-Allmaras with QCR correction), it is interesting to consider some other ones in order to estimate the sensitivity of the computed stall to the model used. The models considered are the Spalart-Allmaras and the k-ω Menter SST [13], QCR correction being applied or not. Let's remind that this correction can be applied to any turbulence model based on Boussinesq's hypothesis, and that it is known to improve the prediction of corner flow [14]. Figure 12 presents the computed $C_L(\alpha)$ curve for the four turbulence models evaluated. As expected, some differences occur on the absolute value of maximum lift, but as a general statement, the results obtained are quite similar. However, there is an interesting behavior observed when considering the QCR correction or not in post-stall regime. There is a kind of plateau observed between α=20° and α=25°for computations without the QCR correction.

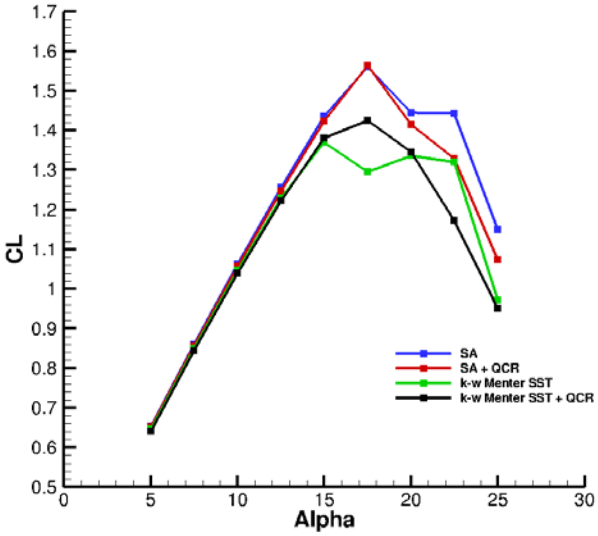

Figure 12 : Effect of turbulence model on $C_L(\alpha)$ curve of the PANDA model.

When considering the computed friction lines in the post-stall regime, similar flow separation patterns are found when QCR correction is active (with one stall cell inboard interacting with the separation at tip) or not (with two stall cells developed on the entire wing span).

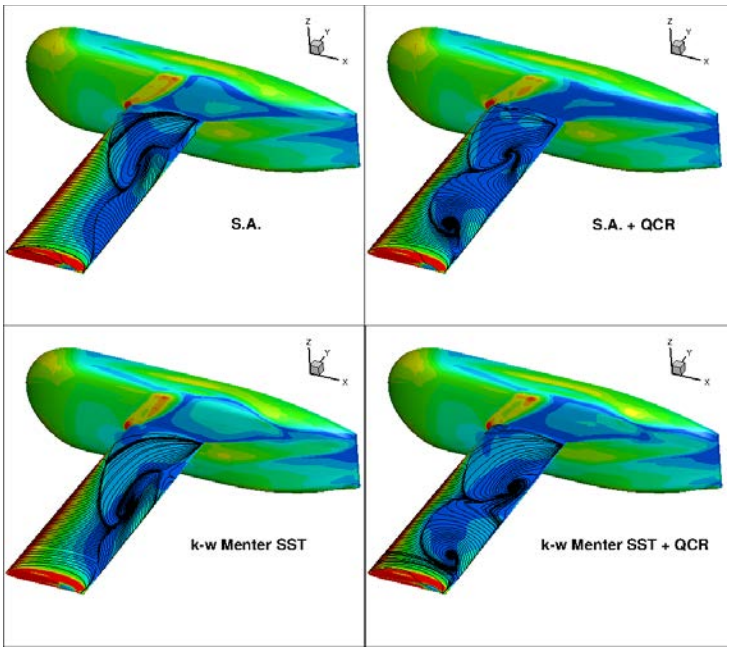

Figure 13 : Computed friction lines for α=22.5°.

When experimental data will be available, some interesting information could be used concerning the validity of turbulence models in the post stall regime.

Effect of leading edge sweep

The model design has to consider the possibility to set the wing at different values of leading-edge sweep angle, positive or negative. At that stage of the design process, only the effect of sweep angle on aerodynamic performance is considered, mechanical details for wing positioning, such as the exact location of rotation axis, being considered later by model workshop. However, due to simple geometrical considerations, the order of magnitude of the extreme sweep angle values can be estimated if a fully integrated solution for wing setting is foreseen. Due to the fuselage height, the wing chord and the space left between tunnel wall and the balance, a sweep angle around $20^o/25^o$ is possible. This value has to be confirmed when model dimensions will be fixed. For this preliminary work, a sweep value of $+/-25^o$ has been considered with a rotation axis located at mid-chord of the root airfoil (Figure 14). Figure 15 compares the computed $C_L(\alpha)$ curves for these three configurations. An estimated $C_L(\alpha)$ curve for an infinite $+/-25^o$ swept wing is drawn for reference.

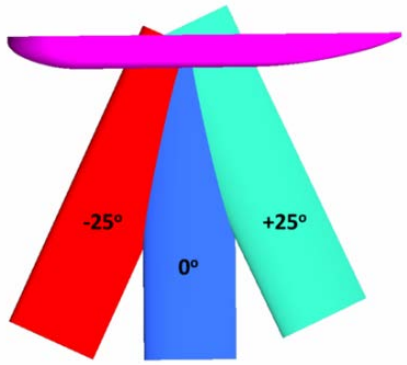

Figure 14 : Swept wing configurations considered.

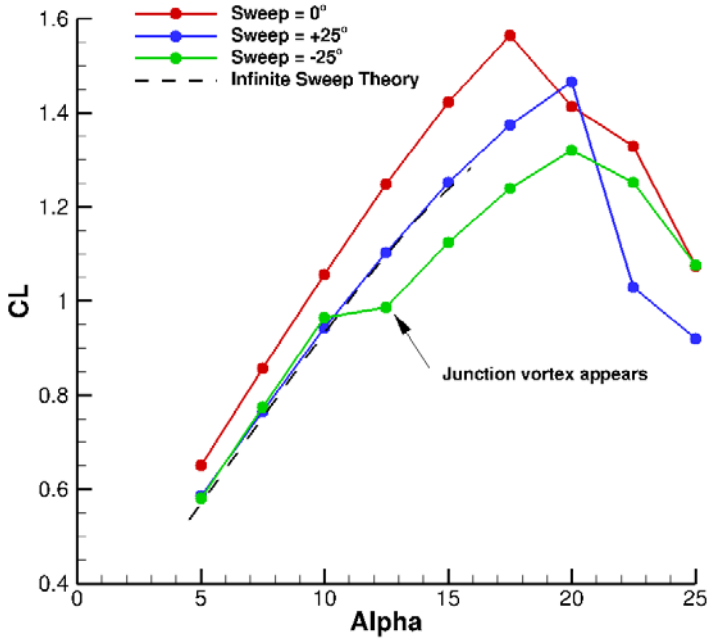

Figure 15 : Computed $C_L(\alpha)$ curves for different sweep angles (V=50m/s, $Re_C=0.904\times10^6$, SA+QCR).

Based on infinite swept wing theory, similar $C_L(\alpha)$ curves should be obtained for both negative and positive sweep values (sweep effect is proportional to cosine of sweep value). This behavior is true up to $\alpha=10^o$, but beyond this incidence, a break in the lift curve is observed for the negative sweep configuration. This is due to the appearance of a junction vortex for this configuration (Figure 16).

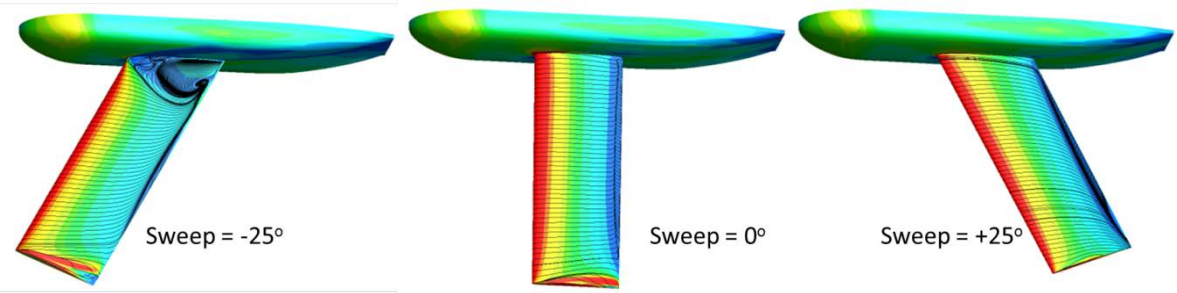

Figure 16 : Effect of leading edge sweep. Computed friction lines at $\alpha=12.5^o$.

It is interesting to note that this vortex has an effect on the wing stall process, as depicted in Figure 17. For the positive sweep configuration, stall process exhibits a more three-dimensional separation line at trailing edge than for the unswept wing case, but with no junction vortex/stall cells.

For the negative sweep case, the stall looks like an interaction between the junction vortex, acting like a "half-stall cell", with the outboard trailing-edge separation, in a similar way to the unswept wing (see Figure 13). These different behaviors will be confirmed/unconfirmed by the experiments.

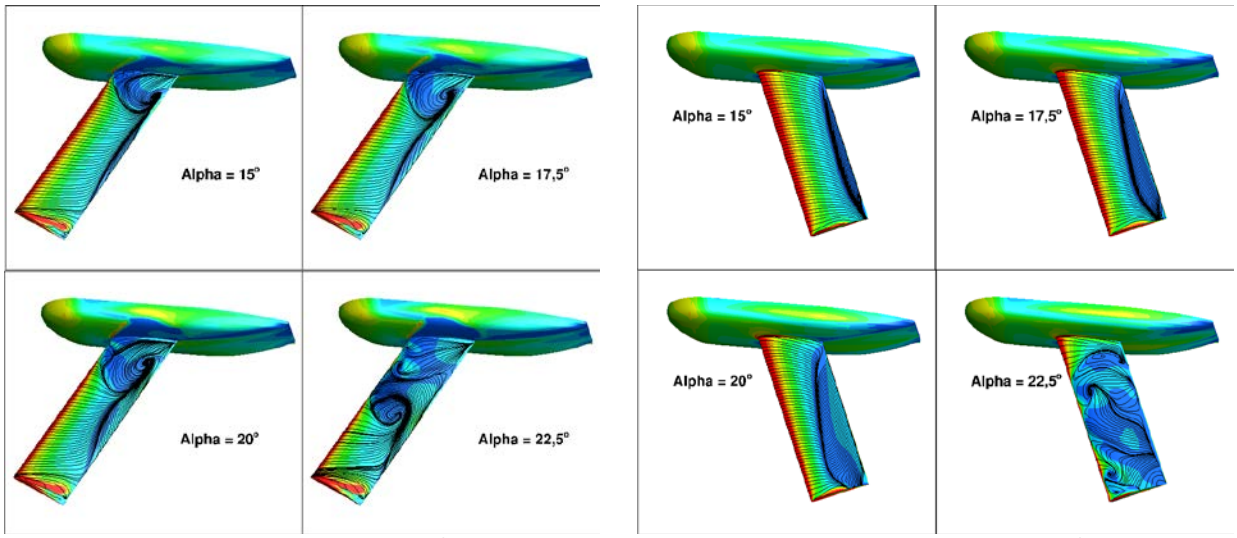

Wing stall for Sweep =-25° Wing stall for Sweep =+25°

Figure 17 : Effect of leading-edge sweep. Computed wing stall process.

Model instrumentation

The number of sensors foreseen for this model dedicated to wing stall study is very high when compared with standard ones. It is made of about 170 static pressure probes and about 50 unsteady ones. Their locations are based on the following principles:

- Static pressure sensors: the objective is to provide Cp distribution on the wing as accurate as possible. Pressure sensors are distributed on both upper and lower surfaces. Five sections of 27 pressure holes are considered (see Figure 18), leading to a total number of 135. A number of 35 sensors remain for other configurations foreseen on this modular model (high lift devices mainly).

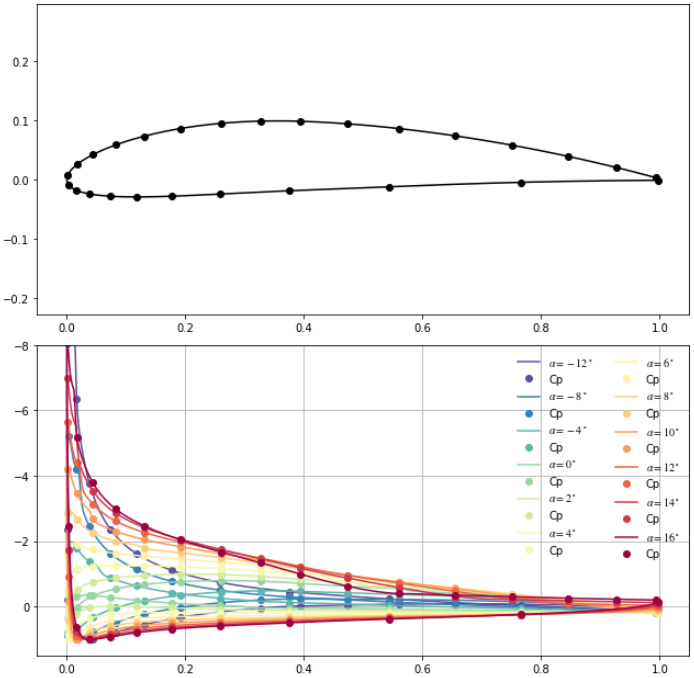

Figure 18 : Static pressure distributions for one wing section.

- Unsteady pressure sensors: these sensors are located on the wing upper surface only. The objective is to catch pressure fluctuations that exist in separated boundary layers, to identify possible stall cells and their spatio-temporal evolution along span. Therefore, four lines of 10 sensors have been considered in the potential zone of interest derived from the computations carried out (Figure 19). A final line has been considered for one section at mid-span.

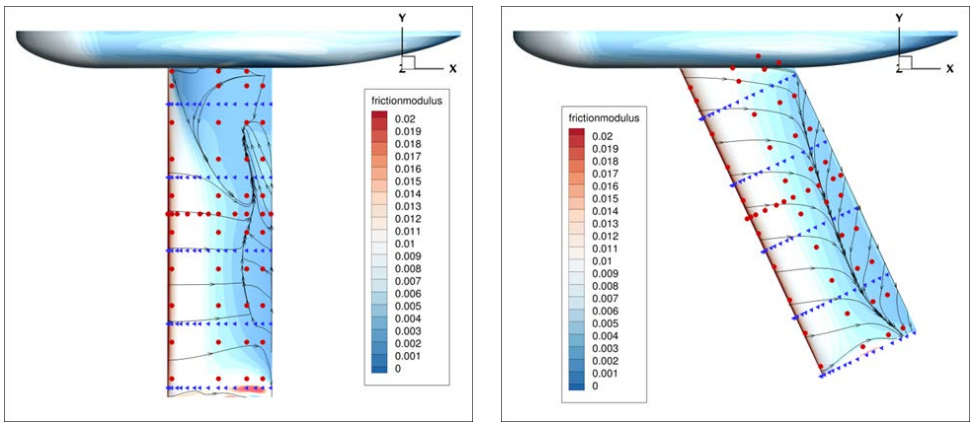

Figure 19 : Sensors locations on wing. Blue: static – Red: unsteady.

The final location of these different sensors will be set once model characteristics will be fixed by the workshop in order to keep all the instrumentation active whatever the configuration tested (see for instance location of unsteady pressure sensors at root for swept wing configuration).

Conclusions

In 2018, ONERA launched an internal research program on wing stall prediction, analysis and control. Among the different tasks of this program, one work package aims at building up experimental database for basic stall phenomena (mainly trailing-edge and leading edge stalls) at low-speed.

A generic model has been designed for these basic researches on wing stall for tests planned in the ONERA-F2 low-speed wind tunnel. The NACA 4412 airfoil has been considered as the baseline for the wing. The twist of the rectangular wing equipped with a generic fuselage has been optimized in order to obtain a quasi two-dimensional flow separation at trailing-edge.

The effect of a leading-edge sweep on performance has been considered, and different stall process have been observed between positive and negative wing sweep values. Finally, a pre-definition of the model equipment (static and unsteady pressure sensors), based on numerical flow solutions, has been defined.

Some remaining design activities are planned to start in 2019, the two main ones being:

- The design of full span flap adapted to the model wing, in order to obtain experimental data for a leading-edge stall;
- The design of a full span slat, for stall driven by wake/boundary layer viscous interactions.

In both cases, the design of flap and slat elements has to minimize the operations on the main wing for configuration changes.

Acknowledgments

The PANDA program is supported by ONERA internal funding. The studies presented in this article are making use of the elsA software funded by ONERA, Airbus and Safran, who are co-owners of this software. The computations presented have been carried out on the ONERA "Sator" HPC machine (NEC). The author thanks the many fruitful exchanges with Prof. Laurendeau, of Polytechnique Montréal, on the overall aerodynamic design of the model.

References

[1] *Loss of Control In-Flight Accident Analysis Report* – IATA Report – 2010-2014 – ISBN 978-92-9252-775-4.

[2] D.A. Crider (NTSB), *"Why are we here?"* ICAO Loss of Control Symposium, Montréal, May 20-22, 2014.

[3] *Statistical Summary of Commercial Jet Airplanes Accidents, Worldwide Operations, 1959-2017*. Published by Aviation Safety, Boeing Commercial Airplanes, October 2018 (http://www.boeing.com/news/techissues/pdf/statsum.pdf).

[4] T.L. Jordan, W.M. Langford, J.S. Hill, *"Airborne Subscale Transport Aircraft Research Testbed – Aircraft Model Development."* AIAA 2005-6432.

[5] C.L. Ladson, C.W. Brooks Jr, *"Development of a Computer Program to obtain Ordinates for NACA 4-digit, 4-digit Modified, 5-Digit and 16-Series Airfoils."* NASA TM X-3284, November 1975.

[6] H. Abbot, A.E. von Doenhoff, L.S. Stivers Jr, *"Summary of Airfoils Data."* NACA Report 824, 1945.

[7] L. Cambier, S. Heib and S. Plot, "*The Onera elsA CFD Software: Input from Research and Feedback from Industry."* Mechanics and Industry, 14(3):159-174, doi:10.1051/meca/2013056, 2013.

[8] A. Jameson, W. Schmidt, and E. Turkel, *"Numerical Solutions of the Euler Equations by Finite Volume Methods Using Runge-Kutta Time Stepping."* AIAA Paper, 81-1259 (1981).

[9] P.R. Spalart, and S.R. Allmaras, *"A One-Equation Turbulence Model for Aerodynamic Flows."* La Recherche Aérospatiale N^{o} 1, 5-21, 1994.

[10] P. R. Spalart, *"Strategies for Turbulence Modelling and Simulation."* International Journal of Heat and Fluid Flow, Volume 21, 2000, pp. 252-263.

[11] *Introduction to ANSYS ICEM CFD HEXA*, Ansys, Inc. http://www.ansys.com/Services/training-center/platform/introduction-to-ansys-icem-cfd-Hexa.

[12] https://hiliftpw.larc.nasa.gov/index-workshop1.html.

[13] F.R. Menter, *"Two-Equation Eddy-Viscosity Turbulence Models for Engineering Applications."* AIAA Journal, Vol. 32, N^{o} 8, August 1994, pp. 1598-1605.

[14] J. Dandois, *"Improvement of Corner Flow Prediction Using the Quadratic Constitutive Relation."* AIAA Journal Vol. 52, N^{o} 12, December 2014, pp 2795-2806.